

Fig. 13. Same as in Fig. 12 from Table II.

resistance of the $n^+p^-n^+$ diode is a very sensitive function of the p^- -region doping level and even a small compensation can increase the resistance dramatically.

REFERENCES

- [1] H. Rees, G. S. Sanghera, and R. A. Warriner, "Low temperature FET for low-power high speed logic," *Electron. Lett.*, no. 6, pp. 156-158, 1977.
- [2] M. S. Shur and L. F. Eastman, "Ballistic transport in semiconductors at low temperatures for low-power high speed logic," *IEEE Trans. Electron Devices*, vol. ED-26, pp. 1677-1683, 1979.
- [3] L. Eastman, R. Stall, D. Woodward, N. Dankekar, C. Wood, M. Shur, and K. Board, "Ballistic electron motion in GaAs at room temperature," *Electron. Lett.*, vol. 16, no. 13, p. 524, 1980.
- [4] R. Zuleeg, "Ballistic effects in current limiters," *IEEE Electron Device Lett.*, vol. EDL-1, Nov. 1980.
- [5] Y. Awano, K. Tomizawa, N. Hashizume and M. Kawashima, "Monte Carlo particle simulation of GaAs submicron n^+i-n^+ diode," *Electron. Lett.*, vol. 18, no. 3, p. 133, 1982.
- [6] M. S. Shur and L. F. Eastman, "Near ballistic electron transport in GaAs devices at 77°K," *Solid-State Electron.*, vol. 24, pp. 11-18, 1981, also in *Proc. Biennial Cornell Conf. Microwave Devices*, Aug. 1979.
- [7] M. S. Shur, "Influence of non-uniform field distribution on frequency limits of GaAs field-effect transistors," *Electron. Lett.*, vol. 12, no. 23, pp. 615-616, Nov. 1976.
- [8] K. S. Knol and G. Diemer, "Theory and experiments on electrical fluctuations and damping of double-cathode valves," Philips Res. Labs., Tech. Rep. 5, pp. 131-152, 1950.
- [9] Amitabh Candra, "Calculation of the free carrier density profile in a semiconductor near an ohmic contact," *Solid-State Electron.*, vol. 23, pp. 516-517, 1980.
- [10] E. H. Rhoderick, *Metal-Semiconductor Contacts*. Oxford, England: Clarendon Press, 1978.
- [11] A. A. Kastalsky and M. S. Shur, "Conductance of small semiconductor devices," *Solid-State Commun.*, vol. 39 (b), p. 715, 1981.
- [12] A. A. Kastalsky, M. S. Shur, and Kwyro Lee, "Conductance of small semiconductor devices," in *Proc. 8th Biennial Cornell Electr. Eng. Conf.*, 1981.
- [13] J. J. Rosenberg, E. J. Yoffa and M. J. Nathan, "Importance of boundary conditions to conduction in short samples," *IEEE Trans. Electron Devices*, vol. ED-28, pp. 941-944, 1981.
- [14] M. A. Hollis, "An investigation of electron transport in two-terminal submicron GaAs devices," M.S. thesis, Cornell University, Ithaca, NY, May 1981.

A Conduction Model for Semiconductor-Grain-Boundary-Semiconductor Barriers in Polycrystalline-Silicon Films

NICKY CHAU-CHUN LU, MEMBER, IEEE, LEVY GERZBERG, MEMBER, IEEE, CHIH-YUAN LU, MEMBER, IEEE, AND JAMES D. MEINDL, FELLOW, IEEE

Abstract—A quantitative trapping model is introduced to describe the electrical properties of a semiconductor-grain-boundary-semiconductor

Manuscript received Feb. 8, 1982; revised August 2, 1982. This work was supported by the Defence Advanced Research Projects Agency under Contract MDA 903-80-C-0432.

N.C.-C. Lu is with IBM Thomas J. Watson Research Center, Yorktown Heights, NY 10598.

L. Gerzberg and J. D. Meindl are with the Integrated Circuits Laboratory, Stanford University, Stanford, CA 94305.

C.-Y. Lu is with the Institute of Electronics, National Chiao-Tung University, Hsin-Chu, Taiwan, Republic of China.

(SGBS) barrier in polysilicon films over a wide temperature range. The grain-boundary scattering effects on carrier transport are studied analytically by examining the behavior of the height and width of a rectangular grain-boundary potential barrier. The model also verifies the applicability of a single-crystal band diagram for the crystallite within which an impurity level exists. Carrier transport includes not only thermionic field emission through the space-charge potential barrier resulting from trapping effects and through the grain-boundary scattering potential barrier but also thermionic emission over these barriers. Thermionic emission dominates at high temperatures; however, at low temperatures, thermionic field emission becomes more important and

the grain-boundary scattering effects are an essential factor. By characterizing the experimental data of the I - V characteristics, resistivity, mobility, and carrier concentration, this model enhances the understanding of the current transport in polysilicon films with grain sizes from 100 Å to 1 μm , doping levels from 1×10^{16} to $8 \times 10^{19} \text{ cm}^{-3}$, and measurement temperatures from -176 to 144°C . The limitations of the model are also discussed.

I. INTRODUCTION

INCREASING INTEREST in applications of polycrystalline silicon (polysilicon) films as photovoltaic and integrated-circuit devices [1], [2] has stimulated a more detailed characterization and understanding of this material. There is a great need for a quantitative model to describe the electrical properties of polysilicon films with different grain sizes and doping concentrations, under various applied biases, and over a wide temperature range. In this paper, a conduction model is introduced to explain the experimental data obtained from polysilicon films with grain sizes of 100 Å to 1 μm , doping concentrations from 1×10^{16} to $8 \times 10^{19} \text{ cm}^{-3}$, under certain bias conditions (applied voltage across each grain $V_g \lesssim 2kT/q$) and over a wide temperature range (from -176 to 144°C). The scattering effects of grain-boundary material on carrier transport are also investigated theoretically and experimentally.

Polysilicon is composed of silicon crystallites with a grain boundary in between two crystallites. Defects caused by incomplete atomic bonding and disordered material in the boundary result in trapping states that reduce the number of carriers and create space-charge regions in the crystallites and a potential barrier that impedes carrier motion [3]. Impurity atoms may also become inactive at the boundary, however, this segregation can be greatly reduced by the appropriate processing conditions and dopant species [4], [5]. To ensure device reproducibility and to focus on carrier transport, boron was chosen in this work as the dopant species, and suitable processing conditions were used to minimize dopant segregation [4], [5]. Earlier trapping models are reviewed in this section, and their inadequacies are discussed.

Kamins [6] considered carrier trapping to explain the mobility behavior in polysilicon. Seto [3] developed the first quantitative derivations to demonstrate the validity of the trapping model. These derivations, however, cannot be applied when the grain is larger than 600 Å and under bipolar bias, because a single and not symmetrical Schottky barrier was used. Biccarani *et al.* [7] varied these derivations to include the possibility that traps may be only partly filled when grains are partially depleted. Both Tarng [8] and Korsh and Muller [9] proposed a symmetrical semiconductor-to-semiconductor junction to explain the I - V characteristics in either oxygen-rich or lightly doped polysilicon films, respectively.

We have modified the above work and demonstrated experimentally the validity of the trapping theory for polysilicon films with grain sizes up to approximately 1 μm , under various applied biases for wide doping levels and above room temperature [4]. A numerical factor $f < 1$ used to modify the effective Richardson constant so as to match the experimental data, however, still lacks satisfactory physical grounds for quantitative characterization [4], [7], [10]. Because we calculated barrier resistivity by taking into account only those carriers

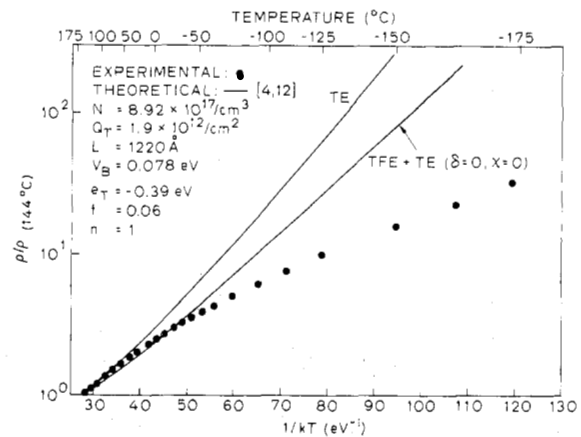


Fig. 1. Measured resistivities normalized at 144°C versus $1/kT$. Theoretical results obtained by the earlier models [4], [12] are also plotted.

with an energy higher than the barrier (thermionic-emission process) but neglecting carriers capable of tunneling through the barrier (thermionic field emission), this model cannot be applied to films operating at lower temperatures. Tarng [8] offered a semiquantitative explanation for this numerical factor f , based on his low-temperature data. Martinez and Piqueras [11] theoretically investigated the influence of thermionic field emission, however, the formula they used to calculate the tunneling probability showed no difference from the formula for metal-semiconductor Schottky barriers.

We developed a model based on both thermionic and thermionic field emission for a symmetrical semiconductor-to-semiconductor junction [12] and demonstrated that thermionic field emission is significant at room temperature and dominant at low temperatures. By including both components, the calculated resistivities improve at reduced temperature, however, they are much higher than experimental results at low temperatures, as demonstrated in Fig. 1. To fit the experimental data over a wide temperature range, it was necessary to include an additional numerical factor $n \geq 1$ in the potential barrier height terms, which means that effective barrier height based on the I - V characteristics is smaller than the calculated values [8], [10]. It is possible that an additional current component exists even after including thermionic field emission; it is also possible that f is much enhanced at low temperatures. Because there is no concrete physical basis for these f and n factors, there is no systematic approach to characterize them.

In films with a grain size smaller than 500 Å above room temperature, the thermionic-field-emission component is greater than the thermionic-emission component, however, it was neglected in most of the earlier models [3], [4], [6], [10], [13]. For example, in films with a grain size of 200 Å [3], the ratio of thermionic-field-emission component to thermionic-emission component is 1.32 at 25°C and at a doping concentration of $1.58 \times 10^{18} \text{ cm}^{-3}$. Calculations including both components, however, cannot yield better agreement with experimental data above room temperature than do calculations based on thermionic emission only (Fig. 1); thermionic emission should be the dominant transport process under the above conditions. This paradox plus the behavior of

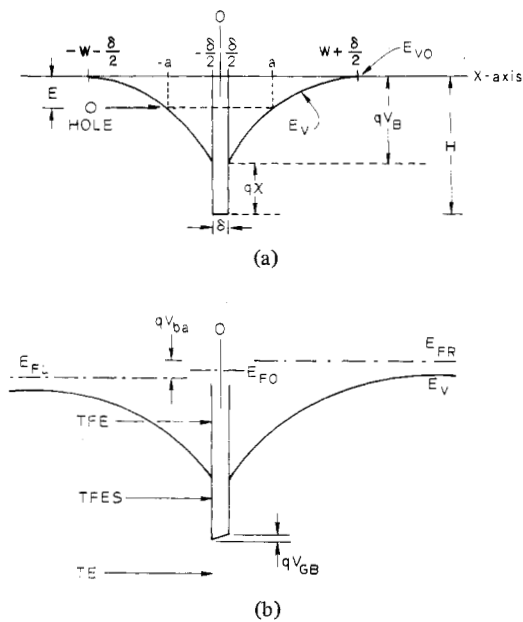


Fig. 2. Potential-energy diagram of a polysilicon grain with p-type dopants. (a) Zero bias. (b) Under bias, showing different components of carrier transport across the barriers.

resistivity at low temperature imply that thermionic field emission should be smaller than predicted by theory [12] above room temperature although it should not be neglected as it has been in the literature [3], [4], [6], [13] as an assumption, and that the total current must be greater at low temperature.

Another inadequacy in the existing models is that the effect of the grain-boundary material on carrier transport has not been quantitatively accounted for in polysilicon films and, because it does exist, it should be included [13]–[15] and characterized. In polycrystalline metal films, for example, the grain-boundary material was addressed as a scattering center and revealed its importance [14].

In this paper, the limitations of the above models are solved by a conduction model wherein a rectangular potential barrier represents the grain-boundary scattering effect [13]–[15] between two space-charge potential barriers resulting from the grain-boundary trapping [3], [4], [6]–[10]; it also calculates thermionic-field-emission and thermionic-emission transport across these barriers (Fig. 2). By using the WKB transmission approximation and the Maxwell-Boltzmann statistics, an analytical J - V expression is derived in normalized closed form over a wide temperature range where the thermionic-field-emission components dominate at low temperature and the thermionic-emission component becomes significant at high temperature. In addition, the f and n factors are replaced by physical parameters—the scattering barrier height χ and its width δ [15]. In this model, the thermionic-field-emission current is drastically reduced above room temperature because of a finite grain-boundary width; below room temperature, total current becomes greater than expected because of a lower χ and δ as the result of less scattering strength. Replacing f and n with these parameters generates a more systematic and wider background for the study of the grain-boundary scattering effects. Detailed theoretical derivations and analyses,

evaluation of assumptions, and limitations of this conduction model are described, and additional experimental data (such as average carrier concentration and mobility at low temperatures) [15] are obtained to support this theory.

II. THEORY

The new conduction model is simplified by the following assumptions and approximations; their validity and limitations will be demonstrated in Section V.

1) Polysilicon is composed of identical cubic grains with a grain size L [3]–[13].

2) The grain boundary contains Q_T (cm^{-2}) traps that are initially neutral and become charged at a certain monoenergetic level E_T (referred to E_{V0}) or e_T (referred to the valence-band edge at the boundary) after trapping the carriers [3], [4], [7]; E_{V0} is the valence-band edge at the center of the grain and is chosen to be a zero electronic energy—negative for upward and positive for downward directions.

3) The single-crystal energy band is applicable inside the crystallites. Doped impurity atoms enter the crystallite lattice substitutionally and are assumed to be uniformly distributed throughout the film after subsequent thermal treatment. The possibility of dopant segregation to the grain boundary was minimized by the proper processing conditions [4]. An impurity level is formed inside the crystallite and impurity atoms are ionized to create majority carriers [4].

4) The abrupt depletion approximation is used for the space-charge potential-barrier calculation [3], [4], [7], [10].

5) An image-charge force, which lowers the barrier height in metal-vacuum and metal-semiconductor junctions [16], is neglected in the semiconductor-grain-boundary-semiconductor (SGBS) junction. It is expected to gradually decrease in the sequence of metal-vacuum/metal-semiconductor/metal-insulator-semiconductor/SGBS junctions because of the similarities in the interfaced materials and symmetry. Even in metal-semiconductor barriers, the image force barrier-lowering effect can be neglected because its magnitude is not of first order [17], [18].

6) One-dimensional majority-carrier transport is assumed, and any contribution from the injection of minority carriers is neglected as is the nonvertical incidence of carriers to the grain boundary. The equivalent carrier effective mass of single-crystal silicon is used in the barriers.

7) The scattering effect of the grain boundary on carrier transport is approximated by employing a rectangular barrier with a width δ and height χ above the space-charge potential (Fig. 2). The effects of image forces on this interfacial potential barrier [19], [20] should not be overemphasized because it was verified [19] that the interface-layer transmission coefficient is approximately given by the nominal values of δ and χ for films with the ratio of interface-layer permittivity to that in free space = 4 and $\delta \geq 10 \text{ \AA}$ [18]. In addition, a rectangular barrier is highly idealized and serves only as a guide to examine the grain-boundary scattering effects [14], [18]. The δ value represents the effective thickness of the electrical scattering range between two grains in the transitional region and has a certain correlation with the metallurgical grain-boundary thickness.

8) The time-independent WKB approximation [21], [22] is used to calculate the transmission coefficient through the space-charge and grain-boundary potential barriers. Its applicability has been comprehensively studied [23], [24] and will be discussed in Section V.

9) The transmission coefficient is assumed to be unperturbed and constant under small applied bias.

10) The Maxwell-Boltzmann statistics (instead of the Fermi-Dirac function) are used to calculate the distribution of majority carriers in energy.

11) The applied voltage V_a over all N_g grains between two resistor contacts is assumed to be equally dropped across all grains. Each grain voltage falls in series across the grain-boundary material, space-charge potential barrier, and crystallite bulk if the grain is not totally depleted.

Fig. 2 is the potential-energy diagram of a polysilicon grain with p-type dopants. The traps in the grain boundary charged by trapping mobile carriers, deplete the regions in the crystallites, thereby, forming potential barriers on both sides of the grain boundary [3], [4]. By using the abrupt depletion approximation and neglecting image force, the space-charge potential is parabolic and is defined as

$$V(x) = V_B \left(1 - \frac{|x| - \delta/2}{W}\right)^2, \quad \delta/2 \leq |x| \leq \delta/2 + W \quad (1)$$

where V_B is the barrier height of the space-charge potential and W is the depletion width that relates to V_B [4] as

$$W = \sqrt{\frac{2\epsilon V_B}{qN}} \quad (2)$$

where ϵ is the single-crystal permittivity and N is the doping concentration. The grain boundary is an effective scattering center for carrier transport [14] and produces a resistivity in series with resistivities resulting from the space-charge potential barrier and the bulk crystallite [4]. This scattering potential is represented by a rectangular potential barrier with width δ and height χ above V_B , that is

$$V(x) = V_B + \chi = \frac{H}{q}, \quad 0 \leq |x| \leq \delta/2 \quad (3)$$

where H is the energy from E_{V0} to the top of the rectangular potential (Fig. 2).

Based on the one-dimensional time-independent Wentzel-Kramer-Brillouin (WKB) approximation, the transmission probability of a carrier with energy $|E| \leq H$ through the potential barrier $V(x)$ [21], [22] is

$$\tau(E) = \exp \left[-\frac{4\pi}{h} \int_{-a}^a \sqrt{2m^*(qV(x) - E)} dx \right]. \quad (4)$$

Here, a is the classical turning point of carriers with energy E , h is Planck's constant, and m^* is the equivalent carrier effective mass. By substituting (1) and (3) into (4), $\tau(E)$ takes the following form in two carrier-energy regimes. When $|E| \leq E_B$

$$\tau_1(\alpha) = \exp \left\{ -\frac{E_B}{E_{00}} \left[\left(1 + \frac{q\chi}{E_B} - \alpha\right)^{1/2} \frac{\delta}{W} + y(\alpha) \right] \right\} \quad (5a)$$

and, when $E_B \leq |E| \leq H$

$$\tau_2(\alpha) = \exp \left\{ -\frac{E_B}{E_{00}} \left(1 + \frac{q\chi}{E_B} - \alpha\right)^{1/2} \frac{\delta}{W} \right\} \quad (5b)$$

where

$$E_B = V_B$$

$$\alpha = E/E_B$$

$$E_{00} = (qh/8\pi)\sqrt{N/m^*\epsilon}$$

$$y(\alpha) = (1 - \alpha)^{1/2} + \alpha \ln \left[\frac{1 - \sqrt{1 - \alpha}}{\sqrt{\alpha}} \right].$$

It should be noted that a constant of the material E_{00} is smaller by a factor of 2 compared to the value obtained for thermionic field emission in metal-semiconductor Schottky barriers [11], [26]. For carriers with $|E| \geq H$, the transmission probability [21], [22] is

$$\tau_3(\alpha) = 1. \quad (5c)$$

The net current density resulting from a small applied voltage (Fig. 2(b)) [11], [12], [26] is

$$J = J_{L \rightarrow R} - J_{R \rightarrow L} = \frac{A^*T}{k} \left[\int_0^\infty f_L(E) \tau(E) dE - \int_0^\infty f_R(E) \tau(E) dE \right] \quad (6)$$

where k is Boltzmann's constant, the effective Richardson constant $A^* = 4\pi qm^*k^2/h^3$, and $f_L(E)$ and $f_R(E)$ are the probability distribution functions for the occupancy of E by carriers to the left and right of the potential barrier, respectively. The grain voltage V_g is dropped on both the barriers and crystallite bulk. The voltages across the space-charge region V_{ba} and across the grain-boundary layer V_{GB} are assumed to be equally divided on each side of the junction [4], [7]-[11], which is reasonable for small bias but requires modifications at large bias that disturbs the symmetry of the barriers. At the small bias, quasi-equilibrium is assumed, which results in

$$f_L(E) = \frac{1}{1 + \exp \{ [E - E_{F0} - (qV_{ba}/2) - (qV_{GB}/2)] / kT \}} \\ \approx \exp \{ [-E + E_{F0} + (qV_{ba}/2) + (qV_{GB}/2)] / kT \} \quad (7a)$$

$$f_R(E) = \frac{1}{1 + \exp \{ [E - E_{F0} + (qV_{ba}/2) + (qV_{GB}/2)] / kT \}} \\ \approx \exp \{ [-E + E_{F0} - (qV_{ba}/2) - (qV_{GB}/2)] / kT \} \quad (7b)$$

where E_{F0} is the Fermi level at zero bias, and the approximations are based on the assumption of the Maxwell-Boltzmann distribution of the majority carriers. Substituting (7) into (6), separating \int_0^∞ into $\int_0^{E_B}$ + $\int_{E_B}^H$ + \int_H^∞ , and using (5) in the three separate integrals yields

$$\begin{aligned}
 J = & \frac{2A^*T}{k} \exp\left(\frac{E_{F0}}{kT}\right) \sinh\left[\frac{q(V_{ba} + V_{GB})}{2kT}\right] \\
 & \times \left[\int_0^{E_B} \exp(-E/kT) \tau_1(E) dE \right. \\
 & \left. + \int_{E_B}^H \exp(-E/kT) \tau_2(E) dE + \int_H^\infty \exp(-E/kT) dE \right].
 \end{aligned} \quad (8)$$

By changing the integral variable from E to α , this expression becomes

$$\begin{aligned}
 J = & 2A^*T^2 \exp\left(\frac{E_{F0}}{kT}\right) \sinh\left[\frac{q(V_{ba} + V_{GB})}{2kT}\right] \\
 & \times \left[\frac{E_B}{kT} \int_0^1 \exp\left(-\frac{\alpha E_B}{kT}\right) \tau_1(\alpha) d\alpha \right. \\
 & \left. + \frac{E_B}{kT} \int_1^{H/E_B} \exp\left(-\frac{\alpha E_B}{kT}\right) \tau_2(\alpha) d\alpha + \exp(-H/kT) \right]
 \end{aligned} \quad (9)$$

which is an analytical J - V solution in normalized closed form. The first term in the bracket describes the thermionic-field-emission component through the space-charge potential (TFE in the following derivations), the second denotes thermionic field emission through the grain-boundary scattering potential, $TFES$, and the third is the thermionic-emission component TE . If $(V_{ba} + V_{GB}) \ll 2kT/q$, and by using

$$p(0) = n_i \exp\left(\frac{E_g/2 + E_{F0}}{kT}\right) \quad (10)$$

where $p(0)$ is the carrier concentration at the center of the grain [4] and n_i is the intrinsic carrier concentration, the following linear J - V expression is obtained

$$J \approx q^2 p(0) \left(\frac{1}{2\pi m^* kT}\right)^{1/2} (V_{ba} + V_{GB}) (TFE + TFES + TE). \quad (11)$$

Over this linear range, the space-charge barrier resistivity $\rho_B = V_B/(2WJ)$ and $\rho_{GB} = V_{GB}/(\delta J)$. Total resistivity ρ (including ρ_B , ρ_{GB} , and the crystallite bulk resistivity ρ_C which is equal to single-crystal resistivity) is [4]

$$\rho = \rho_B \left(\frac{2W}{L}\right) + \rho_{GB} \left(\frac{\delta}{L}\right) + \rho_C \left(1 - \frac{2W}{L} - \frac{\delta}{L}\right). \quad (12)$$

Substituting (11) into (12) results in

$$\rho = \frac{(2\pi m^* kT)^{1/2}}{Lq^2 p(0)} \left(\frac{1}{TFE + TFES + TE}\right) + \rho_C \left(1 - \frac{2W}{L} - \frac{\delta}{L}\right) \quad (13)$$

which is a general expression for polysilicon resistivity from which the effective mobility of polysilicon μ_{eff} can be calculated [(15) and (16) in the paper by Lu *et al.* [4]]. To calculate

ρ and μ_{eff} , the quantities W , V_B , E_{F0} , $p(0)$, and the average carrier concentration \bar{p} [3], [4] are required for $N \leq N^*$ and $N \geq N^*$, where N^* is a critical doping concentration below which the grains are totally depleted; otherwise, they are only partially depleted [4], [7]. These quantities are derived in detail and the temperature effects on the intrinsic carrier concentration n_i and band gap of crystallites are included [4]. The acceptor impurity level within the forbidden band gap for boron is $E_A = -0.08 + 4.3 \times 10^{-8} N^{1/3}$ [28].

To interpret the I - V measurements and small-signal resistivity in polysilicon films under different experimental conditions, it is necessary to know how such parameters as N , T , χ , and δ affect majority-carrier transport across the barriers. These important analyses will be done in Appendix I.

It is found that TE dominates at high temperatures, where χ and V_B are key factors that impede carrier transport; at low temperatures, TFE is more important and δ and V_B becomes the determinant parameters. Although no simple and exact form was found to correlate $TFE + TFES + TE$ with conventionally used $TE [=f \cdot \exp(-qV_B/nkT)]$, a semiquantitative relationship between them can be approximated, that is

$$\begin{aligned}
 \text{TOTAL} & \equiv TFE + TFES + TE \\
 & \approx \exp(-\chi^{1/\eta} \delta^{1/\lambda}) \exp(-qV_B/nkT)
 \end{aligned} \quad (14)$$

where $\eta \geq 1$ and $\lambda \geq 1$, both of which are functions of temperature and doping concentration, and χ is in volts and δ is in angstroms. Card and Rhoderick [18] simplified their studies of the interface effects in silicon Schottky diodes, based on $\eta = 2$ and $\lambda = 1$; however, from the analysis in Appendix I, this is valid only at high temperatures and very large χ . Equation (14) provides a simple and semiquantitative basis for a comparison between experimental data and theory by adjusting χ and δ .

III. EXPERIMENT

A. Sample Preparation and Measurements

Because the details of sample preparation are similar to those in the paper by Lu *et al.* [4], they are only briefly described in this section. Ring-and-dot resistors, rectangular resistors, four-point-probe pads, and Van der Pauw structures were used for measuring resistivity, mobility, and carrier concentration. Undoped 1.0- μm polysilicon films were deposited on an oxide layer in an atmospheric-pressure CVD epitaxial reactor in an H_2 ambient pyrolysis of silane at 1050°C. A 500-Å (instead of 2000 Å [4]) layer of SiO_2 was used as a cap for annealing at 1100°C after boron implantation and as a mask for polysilicon etching after annealing, if necessary for patterning. Highly doped regions to ensure ohmic contacts were formed either by implantation to avoid wide lateral diffusion or by boron diffusion to make the polysilicon resistors compatible with the bipolar process [27]. Processing was characterized by the α -step for measuring polysilicon and oxide thickness, spreading resistance, and SIMS for checking the dopant-distribution uniformity, scanning electron microscopy (SEM) for examining surface topology, and dark-field transmission electron microscopy (TEM) for measuring grain size and distribution. The results were consistent with those obtained in [4].

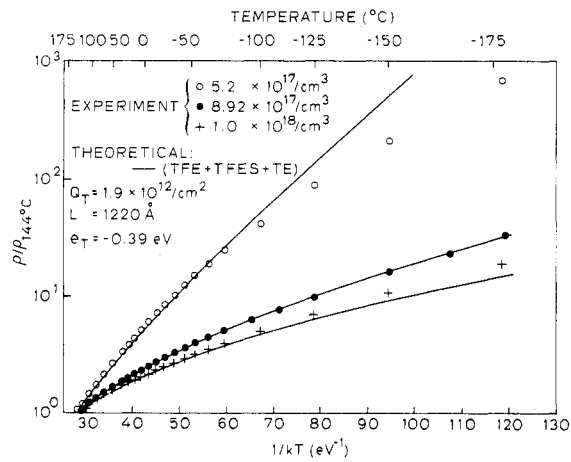


Fig. 3. Measured and theoretical resistivities normalized at 144°C versus temperature at different doping concentrations.

Electrical measurements included the I - V characteristics, resistivity, and Hall voltage. The temperature ranged from 144° to -185°C , which is a near-liquid nitrogen temperature for the I - V and resistivity measurements. The samples were bonded and exposed inside a temperature-controlled oven with an accuracy of $\pm 0.5^\circ\text{C}$. Data taken after each temperature was held constant for at least 1 h ensured thermal equilibrium between the devices and ambient. The same Hall setup as in Lu's research [4] was used, except for a modified sample holder whose temperature can be changed from -150° to 90°C . The limitation of this setup was that the measurement accuracy degraded below acceptable levels when mobility was lower than approximately $5 \text{ cm}^2/\text{V} \cdot \text{s}$.

B. Results

Measured resistivity data normalized at 144°C versus $1/kT$ (eV^{-1}) are plotted in Fig. 3 for various N . Above room temperature, a nearly linear relationship was observed, however, when the temperature was lowered, the curves became nonlinear. There is no single activation energy for resistivity [4] over the entire temperature range, which indicates that, in addition to thermionic emission, other transport processes exist at low temperatures. Although V_B is an implicit function of temperature, it is not strong enough to fully account for this observation.

Measured I - V data with a logarithmic current axis are plotted in Fig. 4 for rectangular resistors with a geometrical length down to $5 \mu\text{m}$ (effective length $\approx 3 \mu\text{m}$) and at room temperature and, in Fig. 5, for a $60\text{-}\mu\text{m}$ resistor at -175 to 144°C . Most of these curves have a hyperbolic-sine behavior, which will be discussed in Sections IV and V.

Fig. 6 plots the ratio of active carrier concentration \bar{p} (measured by Hall effects) to doping concentration versus $1/kT$ at $N = 3 \times 10^{18}$ and $1 \times 10^{19} \text{ cm}^{-3}$. The active carrier concentration drops at low temperature in samples with a doping concentration of $3 \times 10^{18} \text{ cm}^{-3}$, but remains nearly constant at $N = 1 \times 10^{19} \text{ cm}^{-3}$. In boron-doped single-crystal silicon at room temperature, the sample degenerates at $6.5 \times 10^{18} \text{ cm}^{-3}$ [4], [28]; this also occurs in boron-doped polysilicon. In Fig. 7, the measured active carrier concentration versus

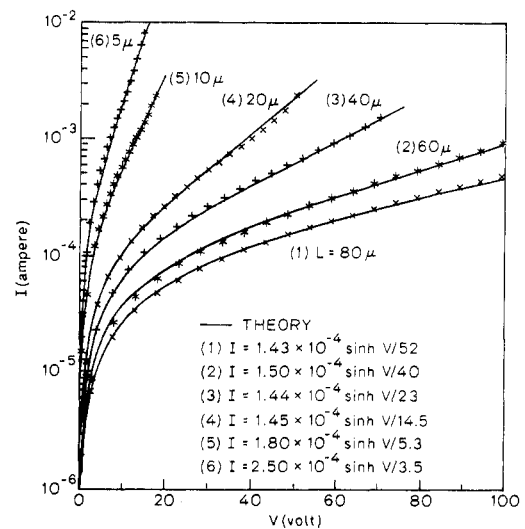


Fig. 4. Measured and theoretical I - V characteristics of polysilicon resistors with lengths from 80 to $5 \mu\text{m}$ and at room temperature.

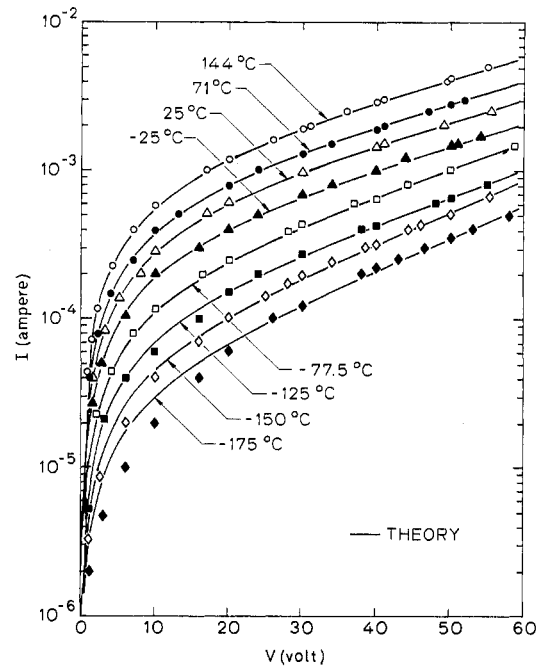


Fig. 5. Measured and theoretical I - V behavior at temperatures ranging from 144 to -175°C . Resistor length = $60 \mu\text{m}$.

doping concentration is shown, where degeneracy again takes place between 5×10^{18} and $1 \times 10^{19} \text{ cm}^{-3}$. A more accurate comparison should include the detailed study on energy-band distortion by heavy doping effects [37].

Experimental hole mobility measured from the Hall effect is plotted in Fig. 8 as a function of $1/kT$ at three doping concentrations. The sample data cannot be completed when $N = 8.92 \times 10^{17} \text{ cm}^{-3}$ at low temperatures because of inaccuracy in the Hall setup. Measured mobility is nearly constant in degenerate samples and no single activation energy appears to exist in nondegenerate films over the entire temperature range. Because mobility excludes the temperature effect of ionized

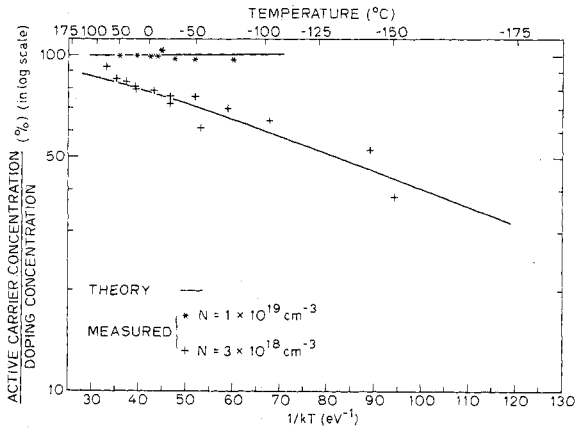


Fig. 6. Measured and theoretical ratios of active carrier concentration to doping concentration versus temperature at two doping levels.

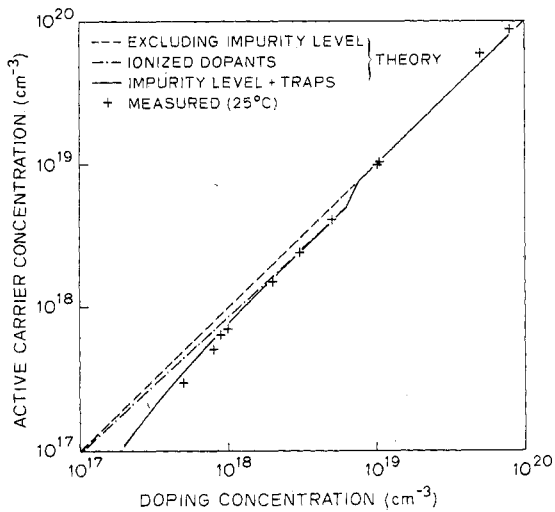


Fig. 7. Measured and calculated active carrier concentrations versus doping concentration at room temperature. The ionized dopant concentrations with and without considering the impurity level are also plotted.

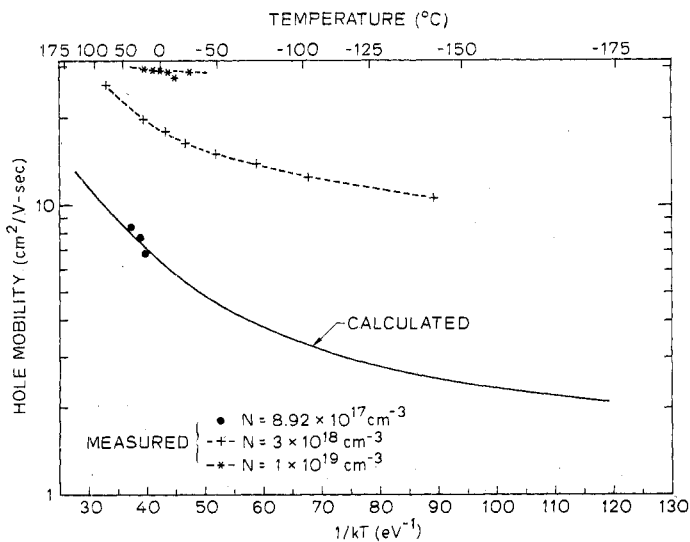


Fig. 8. Measured and calculated hole mobilities versus temperature at three doping concentrations.

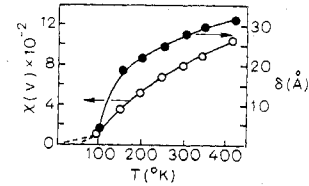


Fig. 9. The values of χ and δ used to match the resistivities in Fig. 3 versus temperature.

dopants in contrast to resistivity, it is another indication of the existence of other important transport processes at low temperature, in addition to thermionic emission.

IV. COMPARISON BETWEEN THEORY AND EXPERIMENTS

To compare theory to the experimental results, it is necessary to determine m^* , ϵ , n_i , E_g , the impurity-level energy E_A , L , Q_T , and e_T . The values of single-crystal silicon were used for the first five parameters [4], [16], [29], and similar procedures were followed to obtain the last three from the experimental data taken above room temperature [4]. ($Q_T = 1.9 \times 10^{12} \text{ cm}^{-2}$, $e_T \approx -0.39 \text{ eV}$, $L = 1220 \text{ \AA}$). This is valid because, above room temperature, TFE is less than 5 percent of TOTAL (Fig. 16) and, based on the $TFES$ and TE components, $\chi^{1/\eta} \delta^{1/\lambda}$ (equivalent to the f factor) has little temperature sensitivity.

A. Small-Signal Resistivity

Both theoretical and experimental results for resistivity versus $1/kT$ from -176 to 144°C and at different doping concentrations were plotted in Fig. 3. From N , Q_T , e_T , and L , V_B was calculated [4] and compared to the measured activation energy of ρ versus $1/kT$ above room temperature, and the results were satisfactory. The plots of χ and δ versus temperature in Fig. 9 were used to fit the data.

When the temperature is reduced, the values of χ and δ , whose products represent scattering strength [14], drop because there must be less phonon scattering in the grain boundary. This observation is strongly supported both experimentally and theoretically in studies of mobility versus temperature in GaAs, Si, and Ge from -173° to 227°C [30] and in polar crystal semiconductors [31]; it is also supported theoretically in studies of electron-optical phonon scattering in the semiconductor-metal-semiconductor structures [32]. In Fig. 1, the theoretical results based on only thermionic emission [3], [4] are in agreement with the experimental data above room temperature, but they deviate below it; in the earlier model that includes both the TE and TFE components [12], normalized resistivity is too low at high temperatures but it improves at reduced temperature, where $f = 0.060$ and $n = 1$. Very close agreement with the measured data has been achieved based on the model developed in this work, however, an exact fit of the data by adjusting χ and δ should not be overemphasized. Of importance is that the functional form of $\rho/\rho_{144^\circ\text{C}}$ versus $1/kT$ based on this work agrees with the experimental data (the curve bends downward) as long as χ and δ decrease at low temperatures. This tendency cannot be achieved in the earlier models and is an indication of the applicability of this conduction model.

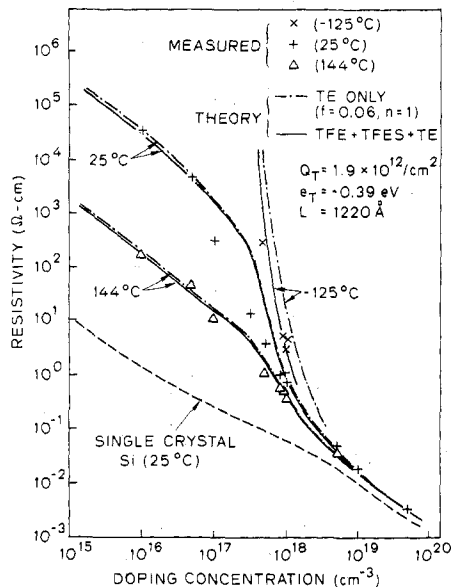


Fig. 10. Measured and theoretical resistivities versus doping concentration of polysilicon films at different temperatures.

Fig. 10 plots the theoretical and experimental resistivities versus doping concentration of polysilicon with a grain size of 1220 Å at the three temperatures. Based on the values of χ and δ in Fig. 9, the theoretical results obtained by this conduction model are in better agreement with experiments at low temperature than are those obtained by the earlier models. Above room temperature, they also demonstrate the same agreement as achieved by the model using the thermionic emission that must include, however, the numerical factors f and n [3], [4].

B. Active Carrier Concentration

The calculated percentage of active carrier concentration to doping concentration versus $1/kT$ was plotted in Fig. 6. The agreement with measured values proves the existence of an impurity level and verifies the assumption of a single-crystal silicon energy band inside the crystallites. This indicates that the energy band of the crystallites is only slightly perturbed in contrast to the proposed potential-fluctuation model [33], [34].

Other evidence can be obtained by plotting the theoretical average carrier concentration versus doping concentration to compare to the experimental data in Fig. 7. The partial ionization of dopants caused by the existence of an impurity level is important at high doping levels and low temperatures. For example, in Fig. 6, more than 50 percent of the dopants were frozen at -150°C and, in Fig. 7, approximately 16 percent were unionized at a doping concentration of $1 \times 10^{18} \text{ cm}^{-3}$ but less than 10 percent of the carriers were trapped at room temperature.

C. Hole Mobility

Fig. 8 shows that the functional form of calculated mobility versus $1/kT$ agrees with experimental data.

D. I - V Characteristics

The following equation was proposed for correlating the small-signal resistance with large-biased I - V characteristics and for verifying its hyperbolic-sine behavior as predicted by theory [4]:

$$I \approx \left(\frac{2\zeta N_g kT}{qR} \right) \sinh \left(\frac{qV_a}{2\zeta N_g kT} \right) \quad (15)$$

where R is the small-signal resistance, V_a is the applied voltage, N_g is the number of grains between the resistor contacts, and ζ is a fitting factor. By measuring R at temperature T , $\zeta \cdot N_g$ can be determined by fitting the large-signal I - V data. Because N_g is proportional to the length of the resistor, the hyperbolic-sine behavior can be properly scaled by scaling the device length (Fig. 4). Below a device geometry of 5 μm , however, it deviates slightly but the I - V relationship still obeys the hyperbolic-sine. Ideally, $\zeta \cdot N_g$ should be constant for a specific-length resistor and independent of temperature. When the temperature is varied, the hyperbolic-sine I - V is observed over a wide temperature range until below approximately -125°C . At lower temperatures, the hyperbolic-sine holds at medium or large bias but not at both. In Fig. 5, the theoretical curve was matched to the large-signal I - V data at temperatures below -125°C . The fitting value of $\zeta \cdot N_g$ (called the effective number of grains) increases as temperature decreases. Similar behavior in oxygen-rich polysilicon was observed by Tarnag [8]; no satisfactory quantitative calculations have been derived, however, to explain this observation. It was believed to be the result of non-uniform grain sizes [8]. This inadequacy is being investigated [44].

V. DISCUSSION

In this section, the validity of the assumptions on which this work was based is investigated and related to their limitations.

Our use of a single-value grain size and uniform grain boundaries is obviously not possible in the real material, although these assumptions are inherently employed in most of the existing models of multigrain polysilicon films in integrated circuits [3]-[13]. This first-order approach is widely accepted because it is simple and efficient in addressing the essential features of polysilicon films. The effects of grain-size distribution and grain-boundary variations are hopefully taken into account by detailed statistical modeling in the future [44]. It is worth to reemphasize, therefore, that the importance of this model is to describe the correct parametric dependencies on experimental data instead of the absolute fitting.

Many possible energy distributions of the trapping states and their effects to the electrical properties of polysilicon have been discussed [7], [36], [40]. Although the δ -function approximation of trapping-state density obtains better results than continuous distributions [7], it is likely that the trapping states are distributed over a specific energy range. In n-type polysilicon it is believed that the grain boundary has an electron trapping center located between the intrinsic Fermi level and the conduction band edge [3], [10]. Recently, there is an experimental observation in favor of a U-shaped trap distribution at the grain boundary [35], [36], where the density

increases rapidly on both sides of intrinsic Fermi level. The trapping-state density of this work is an average value extracted from thermal properties of polysilicon resistors and has slight variations with doping concentration [3], [4], [38].

The validity of the WKB tunneling probability approximation has been studied theoretically and experimentally by Gundlach and Simmons [24]. They developed a specific criterion to evaluate the degree of the approximation with an exact transmission coefficient from the solution of the Schrödinger equation. If the product of the distance between the classical turning points (in angstroms) and the square root of the mean barrier height (in volts) is greater than 4, the results obtained from the WKB approximation have the same exponential forms as those from the exact solution; they differ only in the pre-exponential factor which is a slowly varying function of barrier parameters and is normally on the order of unity. For a slowly changing potential at the turning points, the results obtained from the approximation and the exact solutions are nearly identical. Even for a rectangular barrier that is expected not to be valid because of its rapid changes in potential, the WKB approximation does yield an acceptable result [24]; the maximum error compared to the exact value of the transmission coefficient is less than 4 percent and decreases rapidly with increasing agreement with the criterion. As a result, the WKB approximation can be applied for any barrier if the above criterion is satisfied, and this is true for polysilicon barriers over most doping and temperature ranges. The functional form of J - V and ρ versus temperature, therefore, is little affected by the WKB approximation. In practice, the criterion cannot be met under such a rare condition as a very low temperature and very high or low doping concentrations (small δ , χ , and V_B); however, at low temperatures and high doping, the resistivity of crystallites becomes dominant.

Use of the Maxwell-Boltzmann statistics instead of the Fermi-Dirac function to calculate the energy distribution of carriers is valid [25] if

$$\frac{ph^2}{(2\pi m^* kT)^{3/2}} \ll 1$$

where p is the carrier concentration. The ratio $p/T^{3/2}$, rather than p and T separately, determines the degree of carrier-distribution degeneracy. The Maxwell-Boltzmann statistics are more satisfactory, therefore, either at a lower doping concentration or higher temperature. For example, for a free electron at room temperature, they can be used if the doping concentration is smaller than 10^{19} cm^{-3} ; if smaller than 10^{18} cm^{-3} , they are sufficient when the temperature is higher than 60 K. The criterion becomes more rigid when the effective carrier mass is reduced. In the boron-doped polysilicon, the hole effective mass is approximately 0.386 of the free-electron mass. At $N \approx 1 \times 10^{18} \text{ cm}^{-3}$, the statistics are valid above 144 K, which is consistent with the deviation of the I - V relationship from the hyperbolic-sine behavior below 148 K. Although there may be other reasons for the deviations, the degeneracy of carriers must be one source. The Maxwell-Boltzmann statistics are generally valid for polysilicon over a

wide doping and temperature range; however, at very high doping levels or very low temperatures, the Fermi-Dirac function should be used in (7) and no simple analytical I - V solution as in (8) exists.

Under some extreme conditions, there may be a need for a more accurate solution than those obtained by the WKB approximation and Maxwell-Boltzmann statistics. For example, at very low temperatures and with very light or heavy doping, the exact transmission probability for the rectangular barrier and the Fermi-Dirac function can both be used if $V_B \ll \chi$. Instead of $\tau(E)$ in (4), the exact form of the transmission probability [21], [22], [24] then becomes

$$\tau(E) = \left[1 + \frac{1}{4} \left(\sqrt{\frac{H-E}{E}} + \sqrt{\frac{E}{H-E}} \right)^2 \cdot \sinh^2 \left(\frac{\beta\delta\sqrt{H-E}}{2} \right) \right]^{-1}, \quad E \leq H \quad (16a)$$

or

$$\tau(E) = \left[1 + \frac{1}{4} \left(\sqrt{\frac{H-E}{E}} + \sqrt{\frac{E}{H-E}} \right)^2 \cdot \sin^2 \left(\frac{\beta\delta\sqrt{H-E}}{2} \right) \right]^{-1}, \quad E \geq H \quad (16b)$$

where $\beta = 4\pi\sqrt{2m^*}/h$, and (16b) yields the transmission coefficient by taking into account the quantum mechanical reflection over the barrier in contrast to the coefficient used in (5c).

In the highly doped samples, besides the inclusion of Fermi-Dirac statistics, the energy-band distortion such as energy-gap narrowing, formation of an impurity band, and the disappearance of impurity ionization energy is also important [37]. Our work used a relationship of impurity-energy level with doping concentration based on [28], i.e., $E_A = -0.08 + 4.3 \times 10^{-8} N^{1/3}$ [4]. The band-gap narrowing effect [16], [37], is not included for simplicity. This simple treatment enhances the understanding of properties of heavily doped polysilicon; however, the detailed characterization requires further work to include more accurate band-distortion effects [37].

The measured sinh I - V characteristic indicates that symmetrical division of the applied voltage on both sides of the barriers is appropriate under small and medium biases. Some modifications are required, however, for large bias. For example, because of the relative shift of the valence band and the barrier asymmetry caused by very large bias, the transmission probability and integration limits in (6) are different from those under zero, small, or medium bias. This may be one of the reasons for the existence of the ζ -factor [18], [38]. At the same time, the distribution of the quasi-Fermi level across the grain boundary becomes important as observed by Pike and Seager [39], [40] in their bicrystals of bulk-polysilicon ingot. The prevalence of the sinh I - V relationship under medium to large bias in the CVD multigrain polysilicon layers in [8] and [9] and in this work, however, differs somewhat from the quasi-saturated I - V regime observed in polysilicon ingot samples [39], [40]. This different behavior deserves further study.

Representing the scattering effects of grain boundaries by

rectangular potential barriers is reasonable for polycrystalline metal films; in similar work [41], a model was proposed for electrical resistivity resulting from point-defect scattering and dislocation scattering represented by δ -function potentials. For polysilicon, the grain boundary must be filled with defects, impurities, or amorphous materials, around which the potential barrier must exist microscopically and cause scattering on the carrier transport. These accumulated effects are represented macroscopically by a rectangular potential barrier whose sources can be categorized as phonon scattering, impurity scattering, and scattering resulting from potential fluctuations, and the product of its height and width is a measure of the scattering strength. The product $\chi \cdot \delta$ decreases with lowering temperature; the lower the temperature, the more drastically it is reduced. This observation is supported by calculating the number of phonons; when the temperature is low, this number is proportional to T^3 and, at high temperature, it is proportional to T . In the disordered grain-boundary material with defects, dangling bonds, impurities, or distorted lattice that cause potential fluctuations, the temperature influence on scatterings is dominated by phonon scattering. This tendency is in qualitative agreement with the observations, and the studies of mobility versus temperature in GaAs, Si, Ge, polar semiconductors, and semiconductor-metal-semiconductors are also in agreement. Another approach to the existence of the grain-boundary rectangular potential is to consider it as the edge of the energy band gap of the grain-boundary material [13]. The utility of this concept, however, is not clear because this material cannot be crystalline but must be disordered and, in turn, the energy band gap would not be a determinant for carrier transport. It may be more reasonable to consider this rectangular potential as a mobility gap of the noncrystalline grain-boundary material [15]. The mobility gap of noncrystalline semiconductors has been extensively studied; however, its temperature effects are not exactly understood [42].

From the depletion approximation, the theoretical V_E is in agreement with those obtained by measuring the activation energy of ρ versus $1/kT$ above room temperature [4]. The distribution of free carriers in the space-charge region should be included at N near N^* , especially for very large grains. At very high N , V_B is small and its effect becomes less dominant compared to that in the crystallite bulk.

VI. SUMMARY

This work introduced a quantitative model to describe the electrical properties of a semiconductor-grain-boundary-semiconductor barrier in polysilicon films over a wide temperature range. It verified the applicability of a single-crystal band diagram for the crystallite within which an impurity level exists. It also described a new analytical approach to the study of the grain-boundary effect on carrier transport under different experimental conditions by studying the behavior of grain-boundary potential-barrier height χ and width δ . The electrical properties resulting from the traps in the grain boundary (such as Q_T , e_T , V_B , W , E_{F0} , and $p(0)$) have been studied theoretically and experimentally [4] and were used in this work, however, carrier transport based on thermionic emission only [4] was extended to include both thermionic and therm-

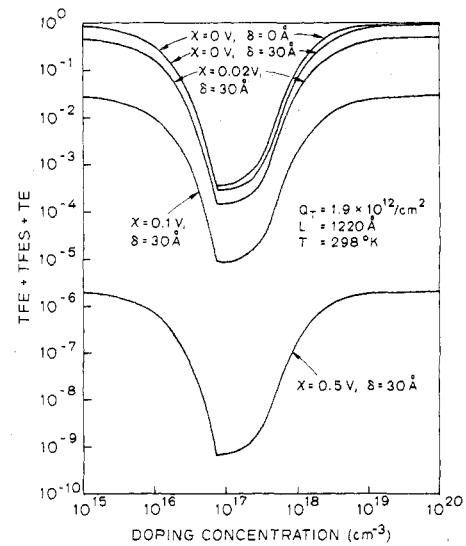


Fig. 11. Calculated room-temperature $TFE + TFES + TE$ versus doping concentration at $\delta = 30 \text{ \AA}$ and with variable χ .

ionic-field-emission processes. By characterizing the experimental data from a combination of these trapping effects and conduction processes, the electrical properties of polysilicon films with grain sizes of less than $1 \mu\text{m}$, doping levels up to $8 \times 10^{19} \text{ cm}^{-3}$, and measurement temperatures from -176° to 144°C can be better understood.

APPENDIX I

Since the effects of χ and δ on current density are shown in (9) only in terms of TFE , $TFES$, and TE , the following analysis is focused on these three components whose sum is designated as TOTAL. The other factor affecting current density is $p(0)$, which is a function of doping concentration [4]. The material parameters $Q_T = 1.9 \times 10^{12} \text{ cm}^{-2}$, $e_T \approx -0.39 \text{ eV}$, $L = 1220 \text{ \AA}$ are used.

A. TOTAL versus N with χ or δ as Variable

In Fig. 11, TOTAL is plotted as a function of doping concentration at room temperature; $\delta = 30 \text{ \AA}$, and χ is variable. The curves are similar but inverted compared to those of V_B versus N [Fig. 10(b), [4]]. Near the critical doping concentration N^* , the high potential barrier impedes carrier transport which, in turn, results in less current. It is important to note that, as χ increases, the curve almost maintains its shape but shifts slightly downward. The reduction of TOTAL caused by a change in χ is a weak function of doping concentration but is a strong function of χ , especially at its large values. Similarly, the change in TOTAL as a result of a variation in χ has little dependence on N , but is a strong function of δ [27]. This simplifies the investigation of the impact of χ and δ on current transport at different temperatures because their effect at a specified doping concentration is a good representative of those under different doping conditions. To simplify this analysis, therefore, the doping concentration was chosen near 5×10^{17} to $1 \times 10^{18} \text{ cm}^{-3}$ for a grain size of 1220 \AA , so that V_B is less sensitive to temperature [Fig. 10(b), [4]] and resistivity is much higher than that of single-crystal silicon.

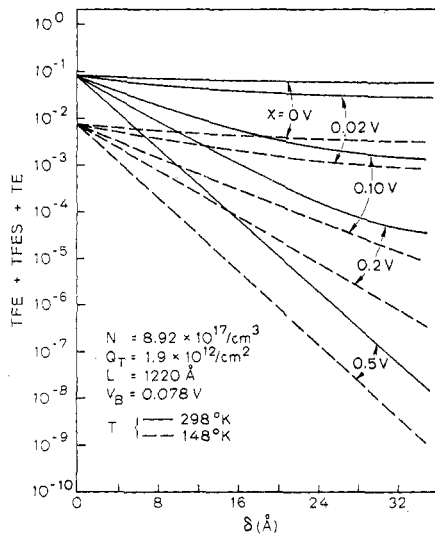


Fig. 12. Calculated $TFE + TFES + TE$ versus δ , with χ as the variable parameter at two temperatures.

B. TOTAL versus δ with Changing χ at Different Temperatures

TOTAL versus δ is plotted in Fig. 12, with $\chi = 0$ to 0.5 V. It can be seen that, at room temperature, TOTAL decreases linearly with increasing δ on a semilogarithmic scale; some curvature appears at intermediate values of χ , however, because TFE , $TFES$, and TE have different dependences on δ . It should be noted that, with the same change of χ , the larger δ produces greater changes in TOTAL; that is, with a wider grain boundary, TOTAL becomes more sensitive to variations of χ . At $\delta = 0$, the effect of χ vanishes, and the results are equivalent to those obtained [12]. When the temperature is lowered to 148 K, TFE and $TFES$ are more important and result in a logarithmic reduction of TOTAL versus δ . At the same χ , TOTAL is smaller at low temperature than high temperature.

C. TFE , $TFES$, or TE versus N with Different χ or δ

Since it is important to understand the interrelationship of TFE , $TFES$, and TE at different values of χ , δ , T , and N , these components are calculated in Fig. 13 as a function of doping concentration at $T = 298$ K, $\delta = 30$ Å, and $\chi = 0.1$ to 0.5 V (TE at $\chi = 0.5$ V is too small to be shown). All three components are sensitive to doping concentrations and are influenced by V_B . The differential amount of each with increasing χ , however, is less sensitive to N which ensures the similar behavior of TOTAL versus N in (a). The results are similar when χ and δ are interchanged. The TE component is independent of δ and remains the same.

D. TFE , $TFES$, or TE versus δ with Changing χ at Different Temperatures

Since the differential amount of TFE , $TFES$, or TE has little dependence on N , these three components versus δ are plotted in Fig. 14 at a doping concentration of 8.92×10^{17} cm⁻³ and at room temperature, with χ varied from 0.02 to 0.05 V. The TE component is very sensitive to χ and can be

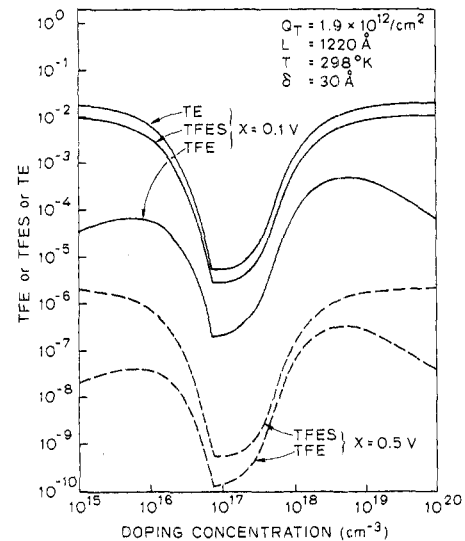


Fig. 13. Calculated room-temperature TFE , $TFES$, or TE versus doping concentration and with variable χ .

reduced by eight decades when χ changes from 0.02 to 0.5 V. The straight lines in the figure indicate that $TFES$ and TFE decrease with δ . Owing to the fact that the TFE , $TFES$, and TE dependences on χ differ, their intersections are varied which implies that, with different χ , their dominant role in TOTAL is interchanged at different δ . TE has no dependence on δ and, as a result, its intersections with TFE and TE determine the cross-points of the curves.

E. TFE , $TFES$, or TE versus χ with Various δ at Different Temperatures

Fig. 15 plots TFE , $TFES$, or TE versus χ , with variable δ at two temperatures. Here, TE is independent of δ and exponentially decreases with increasing χ ; however, TFE and $TFES$ are also reduced but with different functions. As in D, with variations in δ , each component shows its dominance at different χ . At low temperatures, TFE and $TFES$ are more important than TE .

F. Ratio of TFE , $TFES$, or TE to TOTAL versus N at Different Temperatures

Fig. 16 plots the ratio of TFE , $TFES$, or TE to TOTAL versus N at different temperatures; the values of χ and δ are based on the results obtained in Section IV. At room temperature, the importance of carrier transport is on the order of TE , $TFES$, and TFE ; when lowered to 148 K, however, the TE component becomes the least significant. When the space-charge barrier potential V_B is raised with a doping concentration approaching N^* , the TFE /TOTAL ratio increases but the $TFES$ /TOTAL and TE /TOTAL ratios decrease. There are two reasons for this behavior. The first is that there are more carriers with energies smaller than V_B as V_B increases, and these carriers must pass through the barriers via the TFE mode; the second is that TE has the functional form of $\exp(-qV_B/kT)$ and TFE of $\exp(-\int \sqrt{qV_B - E} dx)$ and, therefore, TE reduces much faster than TFE with a rise in V_B .

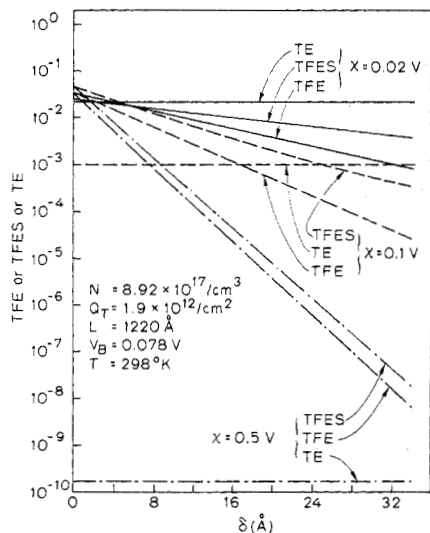


Fig. 14. Calculated room-temperature *TFE*, *TFES*, or *TE* versus δ at different χ .

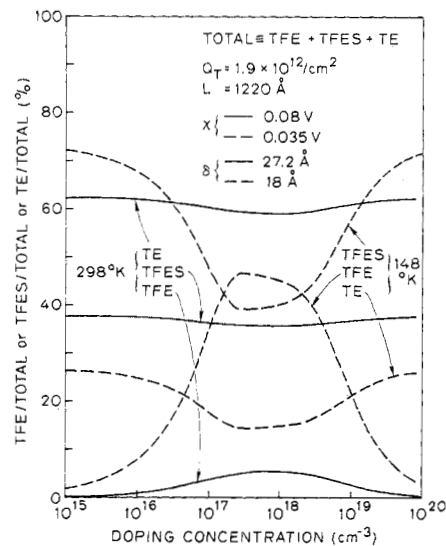


Fig. 16. Calculated ratio of *TFE*, *TFES*, or *TE* to *TOTAL* versus doping concentration at two temperatures.

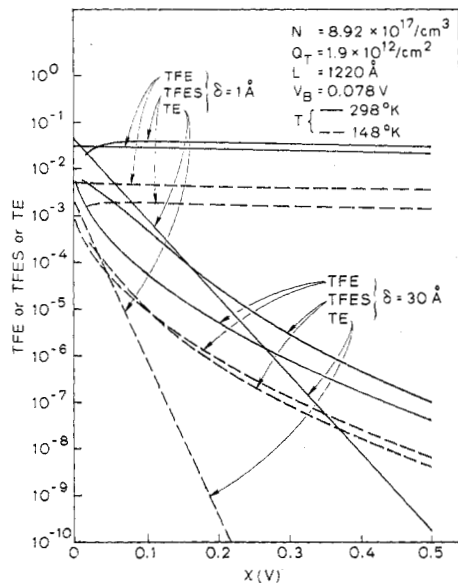


Fig. 15. Calculated *TFE*, *TFES*, or *TE* versus χ and with variable δ at two temperatures.

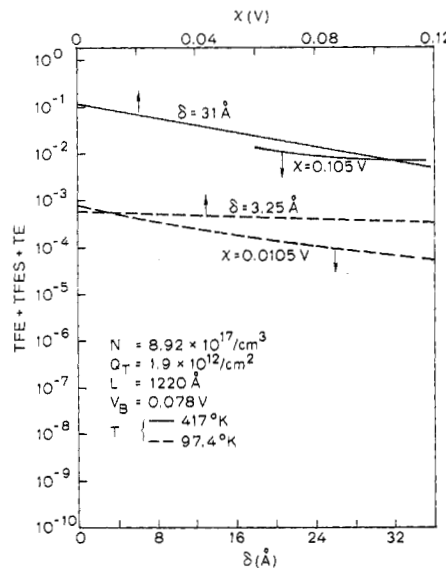


Fig. 17. Calculated *TFE* + *TFES* + *TE* versus χ or δ at two temperatures.

G. Importance of χ and δ to TOTAL at Different Temperatures

In Fig. 17, *TOTAL* is plotted versus χ or δ at two temperatures. At 417 K, the solid lines indicate that *TOTAL* is more dependent on the change of χ than on the variation of δ ; at lower temperatures, however, it is more sensitive to δ than χ . This behavior is obvious by examining (5) and (9) where δ influences the *TFE* and *TFES* values but not the *TE* component and χ affects all three, particularly *TE* and *TFES*. Because, at high temperatures, more carriers are thermally excited to pass over the barriers via the *TE* and *TFES* modes, χ and V_B are determinant for carrier transport. At low temperatures,

carriers that must pass through the barriers via the *TFE* and *TFES* modes are less thermally excited, and δ and V_B play a more important role in carrier flow.

REFERENCES

- [1] L. L. Kazmerski, Ed. *Polycrystalline and Amorphous Thin Films and Devices*, New York: Academic Press, 1980.
- [2] M. L. Hammond, T. I. Kamins, R. S. Muller, and S. P. Murarka, "Polycrystalline-silicon and refractory-silicide films for integrated circuits," Continuing Education in Engineering, University Extension and the College of Engineering, University of California, Berkeley, Apr. 1980.
- [3] J.Y.W. Seto, "The electrical properties of polycrystalline silicon films," *J. Appl. Phys.*, vol. 46, pp. 5247-5254, 1975.

- [4] N.C.-C. Lu, L. Gerzberg, C. Y. Lu, and J. D. Meindl, "Modeling and optimization of polycrystalline silicon resistors," *IEEE Trans. Electron Devices*, vol. ED-28, pp. 818-830, 1981.
- [5] M. M. Mandurah, K. C. Saraswat, C. R. Helms, and T. I. Kamins, "Dopant segregation in polycrystalline silicon," *J. Appl. Phys.*, vol. 51, pp. 5755-5763, Nov. 1980.
- [6] T. I. Kamins, "Hall mobility in chemically deposited polycrystalline silicon," *J. Appl. Phys.*, vol. 42, pp. 4357-4365, 1971.
- [7] G. Baccarani, B. Ricco, and G. Spadini, "Transport properties of polycrystalline silicon-films," *J. Appl. Phys.*, vol. 49, pp. 5565-5570, 1978.
- [8] M. L. Tarnag, "Carrier transport in oxygen-rich polycrystalline silicon films," *J. Appl. Phys.*, vol. 49, pp. 4069-4076, 1978.
- [9] G. J. Korsh and R. S. Muller, "Conduction properties of lightly doped polycrystalline silicon," *Solid-State Electron.*, vol. 21, pp. 1045-1051, 1978.
- [10] N.C.-C. Lu, L. Gerzberg, and J. D. Meindl, "A quantitative model of the effect of grain size on resistivity of polycrystalline silicon resistors," *IEEE Electron Device Lett.*, vol. EDL-1, no. 3, pp. 38-41, 1980.
- [11] J. Martinez and J. Piqueras, "On the mobility of polycrystalline semiconductors," *Solid-State Electron.*, vol. 23, pp. 297-303, 1980.
- [12] N.C.-C. Lu, L. Gerzberg, C. Y. Lu, and J. D. Meindl, "Thermionic field emission in polycrystalline-silicon films," in *Proc. Electrochem. Soc. Fall Meet.* (Hollywood, FL), Abs. no. 528, pp. 1321-1323, Oct. 1980.
- [13] M. M. Mandurah, K. C. Saraswat, C. R. Helms, and T. I. Kamins, "Effects of annealing on the electrical properties of polycrystalline silicon," in *Proc. Electrochem. Soc. Fall Meet.* (Hollywood, FL), Abs. no. 483, pp. 1103-1105, Oct. 1980.
- [14] A. F. Mayadas and M. Shatzkes, "Electrical resistivity model for polycrystalline films: The case of arbitrary reflection at external surfaces," *Phys. Rev. B*, vol. 1, no. 4, pp. 1382-1389, 1970.
- [15] N.C.-C. Lu, L. Gerzberg, C. Y. Lu, and J. D. Meindl, "A new conduction model for polycrystalline silicon films," *IEEE Electron Device Lett.*, vol. EDL-2, no. 4, pp. 95-98, 1981.
- [16] S. M. Sze, *Physical of Semiconductor Devices*. New York: Wiley, 1969, ch. I, IV, VIII; also 2nd ed., 1982, p. 143.
- [17] H. K. Henisch, *Rectifying Semiconductor Contacts*. Oxford, England: Clarendon, 1957.
- [18] H. C. Card and E. H. Rhoderick, "Studies of tunnel MOS diodes," *J. Phys. D: Appl. Phys.*, vol. 4, pp. 1589-1611, 1971.
- [19] J. G. Simmons, "Generalized formula for the electric tunnel effect between similar electrodes separated by a thin insulating film," *J. Appl. Phys.*, vol. 34, pp. 1793-1903, 1963.
- [20] M. Kleefstra and G. C. Herman, "Influence of the image force on the band gap in semiconductors and insulators," *J. Appl. Phys.*, vol. 51, pp. 4923-4926, 1980.
- [21] M. Alonso and H. Valk, *Quantum Mechanics: Principles and Applications*. New York: Wiley, 1973, pp. 181-197.
- [22] A. S. Davydov, *Quantum Mechanics*, 2nd ed. Oxford, England: Pergamon, 1976, pp. 80-86.
- [23] C. Y. Chang and S. M. Sze, "Carrier transport across metal-semiconductor barriers," *Solid-State Electron.*, vol. 13, pp. 727-740, 1970.
- [24] K. H. Gundlach and J. G. Simmons, "Range of validity of the WKB tunnel probability and comparison of experimental data and theory," *Thin Solid Films*, vol. 4, pp. 61-79, 1969.
- [25] R. K. Pathria, *Statistical Mechanics*. Oxford, England: Pergamon, 1972, pp. 132-145.
- [26] C. R. Crowell and V. L. Rideout, "Normalized thermionic-field (T-F) Emission in Metal-Semiconductor (Schottky) Barriers," *Solid-State Electron.*, vol. 12, pp. 89-105, 1969.
- [27] N.C.-C. Lu, "Monolithic polycrystalline-silicon passive devices: Theory, realization, and applications," Ph.D. dissertation, TR no. G549-1, Stanford Electronics Lab., Stanford, CA, Aug. 1981.
- [28] G. L. Pearson and J. Bardeen, "Electrical properties of pure silicon and silicon alloys containing boron and phosphorus," *Phys. Rev.*, vol. 75, pp. 865-883, 1949.
- [29] R. S. Muller and T. I. Kamins, *Device Electronics for Integrated Circuits*. New York: Wiley, 1977, ch. I (Tables 1.1, 1.2).
- [30] F. J. Blatt, *Physics of Electronic Conduction in Solids*. New York: McGraw-Hill, 1968, pp. 259-275.
- [31] F. C. Brown, "Experiments on the polaron," in *Polarons and Excitons*, C. G. Kuper and G. D. Whitefields, Eds. London, England: Oliver and Boyd, 1963, pp. 323-344.
- [32] C. R. Crowell and S. M. Sze, "Electron-optical-phonon scattering in the emitter and collector barriers of semiconductor-metal-semiconductor structures," *Solid-State Electron.*, vol. 8, pp. 979-990, 1965.
- [33] M. Hirose, M. Taniguchi, and Y. Osaka, "Electronic properties of chemically deposited polycrystalline silicon," *J. Appl. Phys.*, vol. 50, pp. 377-382, 1979.
- [34] M. Taniguchi, M. Hirose, Y. Osaka, S. Hasegawa, and T. Shimizu, "Current transport in doped polycrystalline silicon," *Japan. J. Appl. Phys.*, vol. 19, pp. 665-673, 1980.
- [35] S. Hirae, M. Hirose, and Y. Osaka, "Energy distribution of trapping states in polycrystalline silicon," *J. Appl. Phys.*, vol. 51, pp. 1043-1047, 1980.
- [36] H. C. DeGraaff, M. Huybers, and J. G. DeGroot, "Grain boundary states and the characteristics of lateral polysilicon diodes," *Solid-State Electron.*, vol. 25, pp. 67-71, 1982.
- [37] K. F. Berggren and B. E. Sernelius, "Band-gap narrowing in heavily doped many-valley semiconductors," *Phys. Rev. B*, vol. 24, pp. 1971-1986, 1981.
- [38] T. Yoshihara, A. Yasuoka, and H. Abe, "Conduction properties of chemically deposited polycrystalline silicon," *J. Electrochem. Soc.*, vol. 127, pp. 1603-1607, 1980.
- [39] C. Y. Wu, "Interfacial layer theory for the Schottky barrier diodes," *J. Appl. Phys.*, vol. 51, pp. 3786-3789, 1980.
- [40] G. E. Pike and C. H. Seager, "The dc voltage dependence of semiconductor grain-boundary resistance," *J. Appl. Phys.*, vol. 50, pp. 3414-3422, 1979.
- [41] C. H. Seager and G. E. Pike, "Grain boundary states and varistor behavior in silicon bicrystals," *Appl. Phys. Lett.*, vol. 35, pp. 709-711, 1979.
- [42] E. A. Kaner and E. P. Feldman, "Influence of dislocations on electrical conductivity and electromagnetic effects in metal," *Sov. Phys.-Solid State*, vol. 10, pp. 2401-2405, Apr. 1969.
- [43] N. F. Mott, "States in the gap in noncrystalline semiconductors," *J. Phys. C: Solid-State Phys.*, vol. 13, pp. 5433-5471, 1980.
- [44] N.C.-C. Lu, C. Y. Lu, M. K. Lee, and G. Chang, "High-field conduction mechanisms in polycrystalline silicon resistors," in *IEDM Tech. Dig.*, pp. 781-784, 1982.